Available online at www.sciencedirect.com
SCIENCE DIRECT®
Acta Materialia 52 (2004) 1597–1608
Acta MATERIALIA
www.actamat-journals.com

Plastic instability in polycrystalline metals after low temperature irradiation

T.S. Byun *, K. Farrell

Metals and Ceramics Division, Oak Ridge National Laboratory, P.O. Box 2008, 1 Bethel Valley Road, MS-6151, Oak Ridge, TN 37831, USA

Received 23 September 2003; received in revised form 26 November 2003; accepted 2 December 2003

Abstract

The dose dependence of plastic instability behavior has been investigated for polycrystalline metals after neutron irradiation at low temperatures (<200 °C). The analyzed materials consist of 10 body-centered cubic (bcc), 7 face-centered cubic (fcc), and 2 hexagonal close packed (hcp) metals. It was found that the metals after irradiation showed necking at yield when the yield stress exceeded the true plastic instability stress, σ_{IS}, for the unirradiated material. It was also shown that σ_{IS} was almost independent of dose below a critical dose. The critical dose is called the dose to plastic instability at yield, D_C, because at higher doses the material shows necking at yield. The D_C values ranged from 0.002 to 0.2 dpa for bcc and hcp metals, except for a high purity iron, that had a D_C value of 6 dpa; whereas the fcc metals gave generally high values ranging from 0.1 to 40 dpa. It is attempted to explain the dose independence of the plastic instability stress by a straightforward shifting of tensile curves by the appropriate strain corresponding to the radiation-induced increase in yield stress. The dose independence of strain-hardening behavior suggests that radiation-induced defects and deformation-produced dislocations give similar net strain-hardening effects.
Published by Elsevier Ltd on behalf of Acta Materialia Inc.

Keywords: Polycrystalline metals; Irradiation hardening; Plastic instability stress; Dose to plastic instability at yield

1. Introduction

In metallic materials the most common irradiation effects are the increase of strength and loss of ductility [1–9]. Reduction in strain-hardening capability is believed to be a reason for the ductility loss by irradiation [1,3–8], and an explanation for the reduction in strain-hardening rate is the softening effect from the clearance of radiation-induced defects by glide dislocations, so-called channeling [4,7–12]. However, these explanations for irradiation effects on strength and strain-hardening behavior can turn out to be questionable if the stress and strain data are displayed in true stress and true strain units and the data before and after irradiation are compared at a given stress level, not at a given strain level. Mogford and Hull [13] proposed that neutron irradiation has an effect similar to that of plastic deformation on the strain-hardening rate of iron, and Luft [10] demonstrated that prior plastic deformation can induce dislocation channels in unirradiated molybdenum. Furthermore, Ohr [2] showed that the strain-hardening portions of the true stress–true strain curves for irradiated iron can be superimposed on the curves for unirradiated material by shifting them in the positive direction along the strain axis. These observations imply that the strain-hardening behavior at a given stress level is not changed by irradiation. This may be possible if the dislocation–dislocation interactions in unirradiated material and the dislocation-related interactions in irradiated material, such as dislocation-defect cluster interactions and dislocation–dislocation pileup interactions in channels, result in similar net hardening effects at a given stress level, although the details of the interactions might be significantly different.

If irradiation results in little or no change of the strain-hardening behavior at a given stress, the

* Corresponding author. Tel.: +1-865-576-7738; fax: +1-865-574-0641.
E-mail address: byunts@ornl.gov (T.S. Byun).

1359-6454/$30.00 Published by Elsevier Ltd on behalf of Acta Materialia Inc.
doi:10.1016/j.actamat.2003.12.023

irradiated material will show plastic instability or necking at the same true stress as the plastic instability stress of unirradiated material, and consequently, the true plastic instability stress will be independent of dose. Recently, the dose independence of the plastic instability stress has been demonstrated for austenitic stainless steels after irradiation in spallation conditions [5]. If such dose independence of the plastic instability stress turns out to be a common phenomenon for metallic materials, it can be used as a true stress criterion for material failure in design and assessment activities for nuclear systems. The goal of this study is to investigate and generalize the dose dependence of plastic instability behavior.

In this study, the plastic instability behavior has been analyzed for 12 alloys and 7 pure metals, including bcc, fcc, and hcp crystalline structures, after irradiation at low temperatures (<200 °C). It is shown that in these metals the plastic instability stress is almost independent of dose over a limited dose range. The dose to plastic instability at yield, where the material starts to experience necking at yield [5,6], is evaluated by comparing the yield stress–dose curve with the plastic instability stress versus dose curve for each material. It is also suggested that the true plastic instability stress is a property of the base, annealed metal and is independent of hardening measures such as prestraining, precipitation hardening, and irradiation hardening.

2. Experiment and calculation

During the past several years, the authors have investigated mechanical properties for more than 30 commercial and model alloys and pure metals after neutron or neutron and proton irradiation at low temperatures (under 200 °C). In the present study, 24 cases (19 metals) were selected and analyzed, focusing on irradiation hardening and plastic instability behaviors. Four of the 19 metals were irradiated in two or three irradiation experiments, making 24 cases in total. Table 1 includes the chemical compositions of the metals and their heat treatments. Among the 19 metals, the bcc metals consisted of three pure metals (Fe, Nb, and V), a pressure vessel steel (A533B), a bainitic steel (3Cr–3WV), and three ferritic/martensitic (F/M) steels (9Cr–1MoVNb, 9Cr–2WVTa, 9Cr–2WV); the fcc metals were two pure metals (Cu and Ni) and five austenitic stainless steels (316, 316LN, EC316LN, HTUPS316, and AL6XN); the hcp metals were Zr and Zr-4. The tension test data have been generated in multiple research programs using three different types of specimens: SS-3, S-1, and BES/NERI types [4–8,14–16]. Gage section dimensions of the specimens are included in Table 1.

Irradiations were performed at two facilities: the hydraulic tube facility of the high flux isotope reactor (HFIR) at the Oak Ridge National Laboratory and the target area of the Los Alamos Neutron Scattering Center (LANSCE) accelerator at the Los Alamos National Laboratory. Irradiation conditions for tensile specimens are summarized in Table 2, along with test temperature. More detailed descriptions can be found elsewhere [6,7,14–16]. In the HFIR irradiation facility, the tensile specimens were exposed for different periods to achieve target damage levels, and most of the displacement damage was produced by fast neutrons ($E > 0.1$ MeV). The irradiation temperature in the HFIR irradiation facility was estimated to be in the range 60–100 °C. In the LANSCE accelerator, the tensile specimens were irradiated at different target-area locations for different irradiation exposures to protons and spallation neutrons. The kinetic energy of incident protons was 800 MeV and nuclear reactions by the protons produce spallation neutrons. It was shown that a larger contribution to damage was made by protons than by spallation neutrons. Both contributions are included in the displacement per atom (dpa) data in Table 2. The average maximum temperature measured by thermocouples was in the range 60–160 °C during irradiation [15].

All tensile tests were conducted at room temperature in screw-driven machines at crosshead speeds of 0.008 mm s^{-1} for SS-3 and BES/NERI type samples, and 0.005 mm s^{-1} for S-1 type specimens; both speeds correspond to a strain rate of about 10^{-3} s^{-1}. Engineering strain, $e = \Delta l / l_0$, was calculated from the recorded crosshead displacement, Δl, using nominal gauge lengths, l_0: 7.62, 8, and 5 mm for the three specimen types, respectively. Engineering stress, S, was calculated as the applied load divided by initial cross-sectional area before irradiation. True stress, σ, and true strain, ε, up to ultimate load were calculated by the following expressions [5,17]:

$$\varepsilon = \ln(1 + e), \tag{1}$$

$$\sigma = S \times \exp(\varepsilon_P), \tag{2}$$

where ε_P is the plastic component of ε [17]. The true stress at the ultimate tensile strength (UTS) is defined as the plastic instability stress, σ_{IS}.

3. Results and discussion

3.1. Engineering stress–strain curves and the criterion for necking at yield

Figs. 1, 2 and 3 present examples of the dose dependencies of engineering stress–strain curves for bcc, fcc, and hcp alloys, respectively. Although common radiation effects in all three alloys were an increase of

Table 1
Materials, heat treatments, and specimen types

#	Materials	Chemical composition (wt.%)	Heat treatment (in vacuum unless specified)	Specimen type[a]
1	A533B-a	Fe–0.22C–0.25Si–1.48Mn–0.52Mo–0.68 Ni–0.018S–0.012P	Annealed at 880 °C for 4 h and air cooled, tempered at 660 °C for 4 h, reheat at 610 °C for 20 h	BES/NERI
2	A533B-b	Fe–0.22C–0.25Si–1.48Mn–0.52Mo–0.68 Ni–0.018S–0.012P	Annealed at 880 °C for 4 h and air cooled, tempered at 660 °C for 4 h, reheat at 610 °C for 20 h	SS-3
3	A533B-c	Fe–0.22C–0.25Si–1.48Mn–0.52Mo–0.68 Ni–0.018S–0.012P	Annealed at 880 °C for 4 h and air cooled, tempered at 660 °C for 4 h, reheat at 610 °C for 20 h	SS-3
4	3Cr–3WV	Fe–0.091C–0.3Mn–0.09Si–0.009S–0.015P–0.02Ni–3.05Cr–0.24V–0.02Cu–3.01W	Heated for 1 h at 1040 °C in flowing argon and cooled to room temperature in the cold zone; then reheated for 1 h at 760 °C and cooled	SS-3
5	9Cr–1MoVNb	Fe–0.09C–0.36Mn–0.08Si–0.004S–0.008P–0.11Ni–8.62Cr–0.98Mo–0.209V–0.063Nb–0.002Ti–0.013Co–0.03Cu–0.013Al–0.01W	Heated for 1 h at 1040 °C in flowing argon and cooled to room temperature in the cold zone; then reheated for 1 h at 760 °C and cooled	SS-3
6	9Cr–2WVTa	Fe–0.11C–0.44Mn–0.21Si–0.015P–8.9Cr–0.01Mo–0.23V–0.012Co–0.03Cu–0.017Al–2.01W–0.06Ta	Heated for 1 h at 1040 °C in flowing argon and cooled to room temperature in the cold zone; then reheated for 1 h at 760 °C and cooled	SS-3
7	9Cr–2WV	Fe–0.12C–0.51Mn–0.23Si–0.007S–0.014P–8.95Cr–0.01Mo–0.24V–0.012Co–0.03Cu–0.018Al–2.01W	Heated for 1 h at 1040 °C in flowing argon and cooled to room temperature in the cold zone; then reheated for 1 h at 760 °C and cooled	SS-3
8	9Cr–2WVTa	Fe–0.11C–0.44Mn–0.21Si–0.015P–8.9Cr–0.01Mo–0.23V–0.012Co–0.03Cu–0.017Al–2.01W–0.06Ta	Heated for 1 h at 1040 °C in flowing argon and cooled to room temperature in the cold zone; then reheated for 1 h at 760 °C and cooled	S-1
9	Mod. 9Cr–1Mo	Fe–0.092C–0.09Ni–8.32Cr–0.86Mo–0.48Mn–0.15Si–0.055N–0.06Nb–0.2V	Heated for 1 h at 1040 °C in flowing argon and cooled to room temperature in the cold zone; then reheated for 1 h at 760 °C and cooled	S-1
10	Fe-a	(99.995% purity)	Annealed at 600 °C for 1 h	BES/NERI
11	Fe-b	Fe–0.013C–0.018Mn–0.018Ni (99.94% purity)	Annealed at 600 °C for 1 h	SS-3
12	Nb	Nb–0.3Si–0.01Ni–0.06Ni–0.05Ta–0.005C–0.001S (99.5% purity)	Annealed at 900 °C for 1 h	BES/NERI
13	V	V–0.026Si–0.039Mo–0.027O–0.0096N–0.0024C (99.8% purity)	Annealed for 30 min at 900 °C	BES/NERI
14	316-a	Fe–0.059C-1.86Mn–0.57Si–0.018S–0.024P–17.15Cr–13.45Ni–2.34Mo–0.1Cu–0.02Co–0.031N	Annealed at 1050 °C for 30 min	BES/NERI
15	316-b	Fe–0.059C-1.86Mn–0.57Si–0.018S–0.024P–17.15Cr–13.45Ni–2.34Mo–0.1Cu–0.02Co–0.031N	Annealed at 1050 °C for 30 min	SS-3
16	316LN	Fe–10.2Ni–16.3Cr–2.01Mo–1.75Mn–0.39Si–0.11N–0.029P	Annealed at 1050 °C for 30 min	SS-3
17	EC316LN	Fe–12.2Ni–17.45Cr–2.5Mo–1.81Mn–0.39Si–0.024C–0.067N	Annealed at 950 °C for 1 h	S-1
18	HTUPS316	Fe–16.2Ni–13.9Cr–2.46Mo–2.04Mn–0.12Si–0.076C–0.021N–0.15Nb–0. 52V–0.27Ti	Annealed at 1200 °C for 12 min	S-1
19	AL6XN	Fe–24Ni–20.5Cr–6.3Mo–0.4Mn–0.4Si–0.02C–0.22N	Annealed at 1110 °C for 30 min	S-1
20	Cu	Cu–1.6S–0.09Cr–0.22Ni–0.1P–0.27Fe–4.8Ag	Annealed at 450 °C for 30 min	BES/NERI
21	Ni	(99.99% purity)	Annealed at 900 °C for 30 min	BES/NERI
22	Zr-4-a	Zr–1.4Sn–0.015C–0.1Fe–0.001S–0.06O–<0.1Ni–<0.001N	Annealed at 670 °C for 30 min	BES/NERI
23	Zr-4-b	Zr–1.4Sn–0.015C–0.1Fe–0.001S–0.06O–<0.1Ni–<0.001N	Annealed at 670 °C for 30 min	SS-3
24	Zr	Zr–0.0058Hf–0.0056Fe (99.94% purity)	Annealed at 670 °C for 30 min	BES/NERI

[a] Gage section dimensions for SS-3, S-1, and BES/NERI types are $0.76 \times 1.52 \times 7.62$, $0.25 \times 1.2 \times 5$, and $0.25 \times 1.5 \times 8$ mm^3, respectively.

Table 2
Summary for irradiation and testing conditions

#	Materials	Crystal structure	Irradiation facility	Dose range (dpa)	Irradiation temperature (°C)	Test temperature (°C)
1	A533B-a	bcc	HFIR	0–0.89	60–100	25
2	A533B-b	bcc	HFIR	0–1.2	60–100	25
3	A533B-c	bcc	HFIR	0–1.28	60–100	25
4	3Cr–3WV	bcc	HFIR	0–1.2	60–100	25
5	9Cr–1MoVNb	bcc	HFIR	0–1.2	60–100	25
6	9Cr–2VWTa	bcc	HFIR	0–1.2	60–100	25
7	9Cr–2WV	bcc	HFIR	0–1.2	60–100	25
8	9Cr–2VWTa	bcc	LANSCE	0–10.2	60–160	25
9	Mod. 9Cr–1Mo	bcc	LANSCE	0–10.2	60–160	25
10	Fe-a	bcc	HFIR	0–0.79	60–100	25
11	Fe-b	bcc	HFIR	0–1.07	60–100	25
12	Nb	bcc	HFIR	0–0.37	60–100	25
13	V	bcc	HFIR	0–0.69	60–100	25
14	316-a	fcc	HFIR	0–0.78	60–100	25
15	316-b	fcc	HFIR	0–1.2	60–100	25
16	316LN	fcc	HFIR	0–1.2	60–100	25
17	EC316LN	fcc	LANSCE	0–10.7	60–160	25
18	HTUPS316	fcc	LANSCE	0–10.7	60–160	25
19	AL6XN	fcc	LANSCE	0–10.7	60–160	25
20	Cu	fcc	HFIR	0–0.92	60–100	25
21	Ni	fcc	HFIR	0–0.6	60–100	25
22	Zr-4-a	hcp	HFIR	0–0.8	60–100	25
23	Zr-4-b	hcp	LANSCE	0–24.6	60–160	25
24	Zr	hcp	HFIR	0–0.63	60–100	25

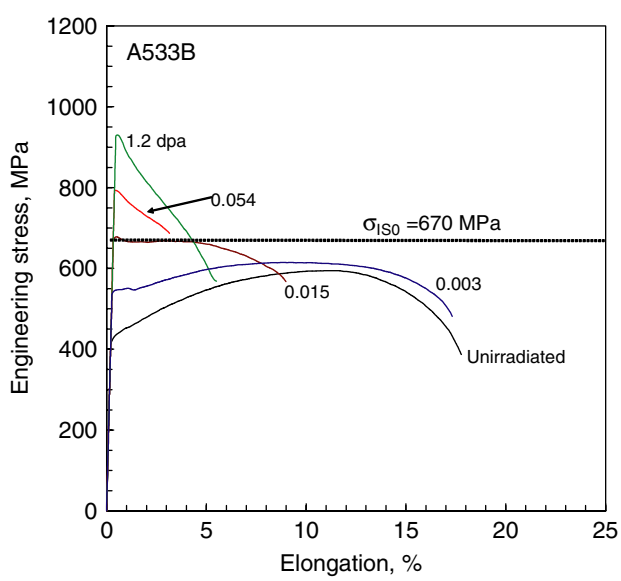

Fig. 1. Engineering stress–strain curves for bcc A533B steel. σ_{IS0} is the plastic instability stress for the unirradiated material.

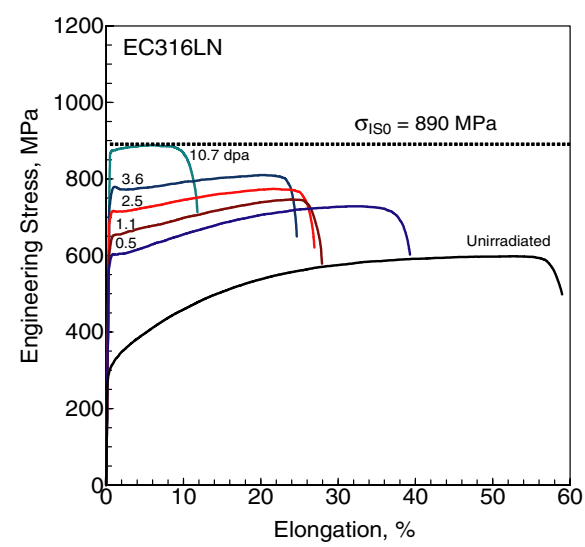

Fig. 2. Engineering stress–strain curves for fcc EC316LN stainless steel.

strength and a decrease of ductility, the details of dose dependence were different for individual alloys. In the A533B pressure vessel steel, the shape of the engineering flow curve changes dramatically as dose increases; both the uniform plastic deformation regime and the necking regime exist in the engineering flow curves before irradiation and at a low dose of 0.003 dpa. However, the uniform plastic deformation regime has disappeared in the curves at higher doses of 0.054 and 1.2 dpa, showing necking at yield. At an intermediate dose of 0.015 the flow curve shows a horizontal region in the strain range 1–4% after a yield drop, which will give a true stress–true strain curve with a slight positive slope.

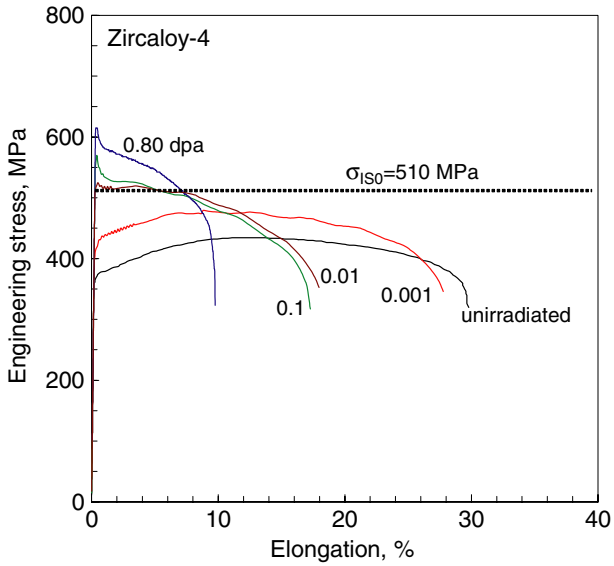

Fig. 3. Engineering stress–strain curves for hcp Zircaloy-4.

In EC316LN stainless steel, the change of curve shape by irradiation was rather progressive up to higher doses, as shown in Fig. 2. This indicates that the fcc material retains significant ductility after severe irradiation; it retained about a 6% uniform strain capability at a high dose of 10.7 dpa. As demonstrated in the next section, the dose level predicted to show a prompt necking at yield is about 22 dpa for the EC316LN stainless steel. This dose level is significantly higher than the dose of 0.015 dpa for A533B steel, however, it is comparable to the dose of 25 dpa obtained form the fusion materials database for 316 stainless steels [1]. Small yield drops are found in the flow curves at medium doses of 1.1 and 2.5 dpa. In irradiated materials, the yield drop can be a sign of channel (or twin) deformation [11,12,16].

The effect of irradiation on the tensile curve of Zircaloy-4 is close to that for the A533B steel, as shown in Fig. 3. The alloy does not show a uniform deformation regime at high doses of 0.1 and 0.8 dpa. At these doses the flow curve shows a significant yield drop of about 30 MPa, followed by a continuous decrease in the engineering stress with strain at a lower rate. The intermediate dose at which the engineering flow curve has a horizontal portion is about 0.01 dpa for this material.

As in our earlier study [5], the plastic instability stress, σ_{IS}, is defined as the critical true stress above which the material shows plastic instability or necking; σ_{IS} is the true stress when the Considere's plastic instability criterion, $\sigma = d\sigma/d\varepsilon_P$ [17], is satisfied. Note that this criterion can be satisfied when there is a yield drop, however, the initial yield drops were ignored in the calculations of σ_{IS}. The calculated true plastic instability stresses of the unirradiated materials prior to necking at yield, σ_{IS0}, are indicated in Figs. 1, 2, and 3; they are 670, 890, and 510 MPa for A533B, EC316LN, and Zircaloy-4, respectively. A noticeable observation concerning the effect of radiation on the tensile flow curve is that the irradiated materials show prompt necking at yield when the yield stress, increased by irradiation, exceeds the σ_{IS0} value for the material. This phenomenon was commonly observed in all alloys analyzed in this study. This means that the true-stress criterion for plastic instability should be dose-independent. This observation led to an extensive analysis of the dose-dependencies of the true plastic instability stress, as described in the following section.

3.2. Dose-dependence of stress parameters

True-stress terms and a critical-dose parameter are defined and described here for use in the following discussion. In the engineering stress–strain curve, there exists a maximum value called the ultimate tensile strength (UTS). The true stress converted from the UTS using Eq. (2) is defined as the true stress at maximum load, σ_{ML}. This true-stress term is also called the plastic instability stress, σ_{IS}, when the specimen shows uniform deformation before plastic instability. If there is no uniform deformation, or prompt necking occurs at yield, σ_{ML} becomes identical with the yield stress (YS or σ_{YS}), which usually occurs after significant irradiation. σ_{IS} is not defined for the cases of prompt necking at yield. Another newly defined term is the dose to plastic instability at yield, D_C [5]. When the irradiation dose, D, exceeds a critical level, the material will deform in a necking mode at the yield point. The critical dose for necking at yield is D_C, which is determined at the intercepting point of the σ_{YS} – dpa curve and the horizontal σ_{IS} – dpa line. Uniform elongation will be virtually zero at any doses above D_C, although the strain during necking can be substantial. In Figs. 4–6, the dose dependencies of the true stress terms σ_{YS} and σ_{ML} (σ_{IS}) are presented for bcc, fcc, and hcp metals, respectively. Since different D_C values were often obtained for an alloy from different programs using different heat-treating facilities, D_C was evaluated for all individual cases and the result is presented in Table 3, along with the plastic instability stresses.

In Fig. 4(a), the dose dependences of σ_{YS} and σ_{ML} are presented for three different cases of an A533B pressure vessel steel. Before irradiation the data of σ_{YS} and σ_{ML} ($=\sigma_{IS}$) were in the ranges 430–520 and 660–750 MPa, respectively. The trend curves show that σ_{YS} increases with dose over the dose range 0–1.2 dpa, while σ_{ML} remains nearly unchanged ($=\sigma_{IS}$) until its trend curve meets with the σ_{YS} curve at a dose of about 0.015 dpa and then it increases with dose. The D_C values were 0.02, 0.015, and 0.02 dpa for A533B-a, A533B-b, and A533B-c cases, respectively. Over the dose range 0–D_C the plastic instability stress σ_{IS} was fairly constant at

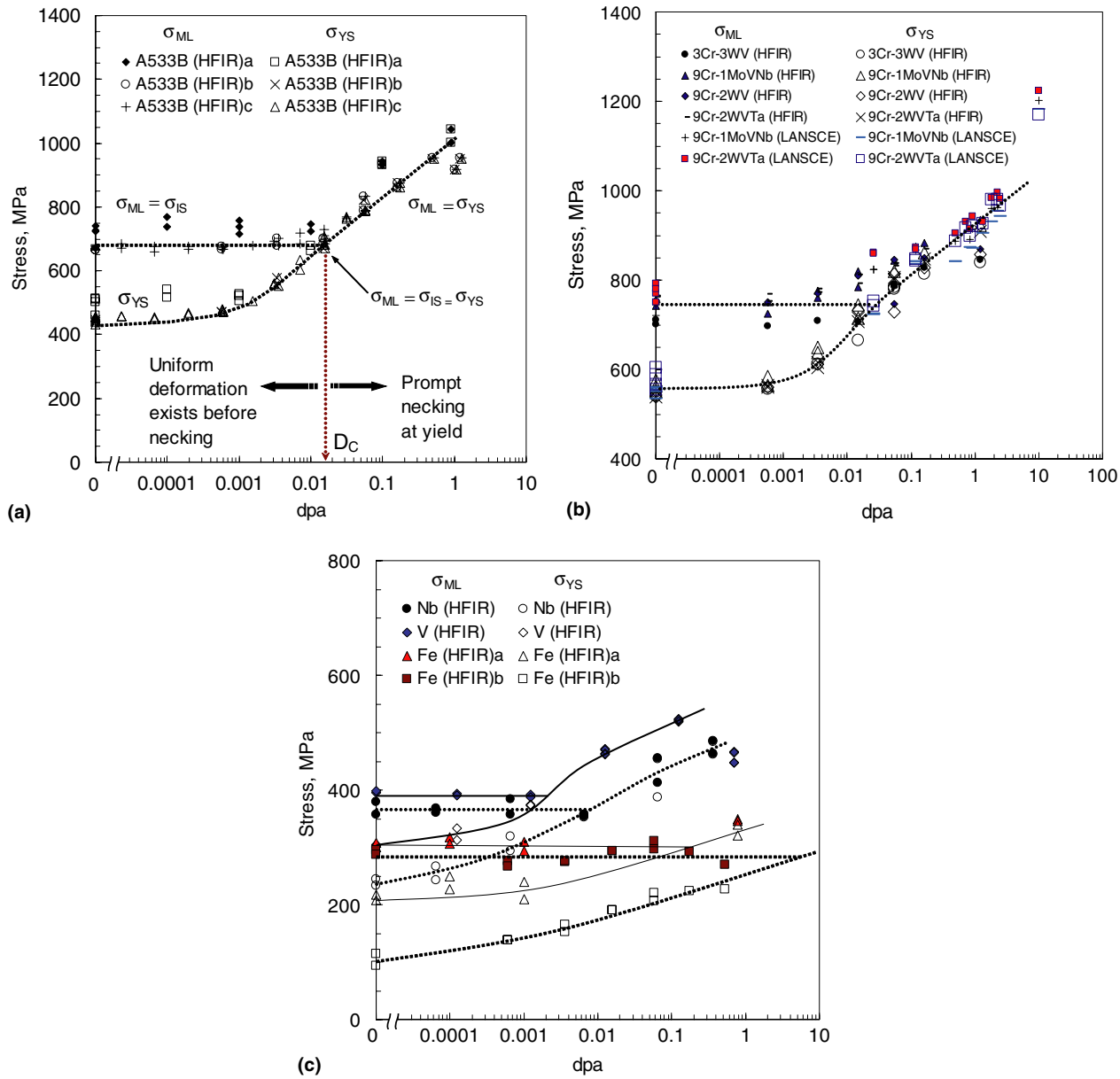

Fig. 4. (a) Dose dependence of the plastic instability stress and yield stress of A533B pressure vessel steel. (b) Dose dependence of the plastic instability stress and yield stress of 3Cr and 9Cr steels. (c) Dose dependence of the plastic instability stress and yield stress of pure bcc metals. Note that Fe-b, V, and Nb are not high purity materials.

about 730 MPa for A533B-a case and at about 680 MPa for the other two cases. It is believed that different cooling rates during heat treatments caused the difference in σ_{IS} values for A533B cases.

After a dose of ~0.015 dpa σ_{ML} became identical with σ_{YS} because necking occurred at yield and both stresses increased with dose. Since a criterion for plastic instability involves plastic deformation only, the deformation in the elastic regime is not relevant to the instability criterion. In the elastic regime of a severely hardened material, therefore, stress can continue to increase and can exceed σ_{IS} before it reaches σ_{YS}. In such a case the deformation regime at yield is already in the midst of plastic instability and σ_{YS} is greater than σ_{IS}; the neck formation in the 'over-stressed' specimen might progress more quickly than in the specimen with large uniform deformation. Relationships among the true stress terms are given by

$$\sigma_{YS} < \sigma_{ML} = \sigma_{IS} \quad \text{for } D < D_C, \tag{3a}$$

$$\sigma_{YS} = \sigma_{ML} = \sigma_{IS} \quad \text{for } D = D_C, \tag{3b}$$

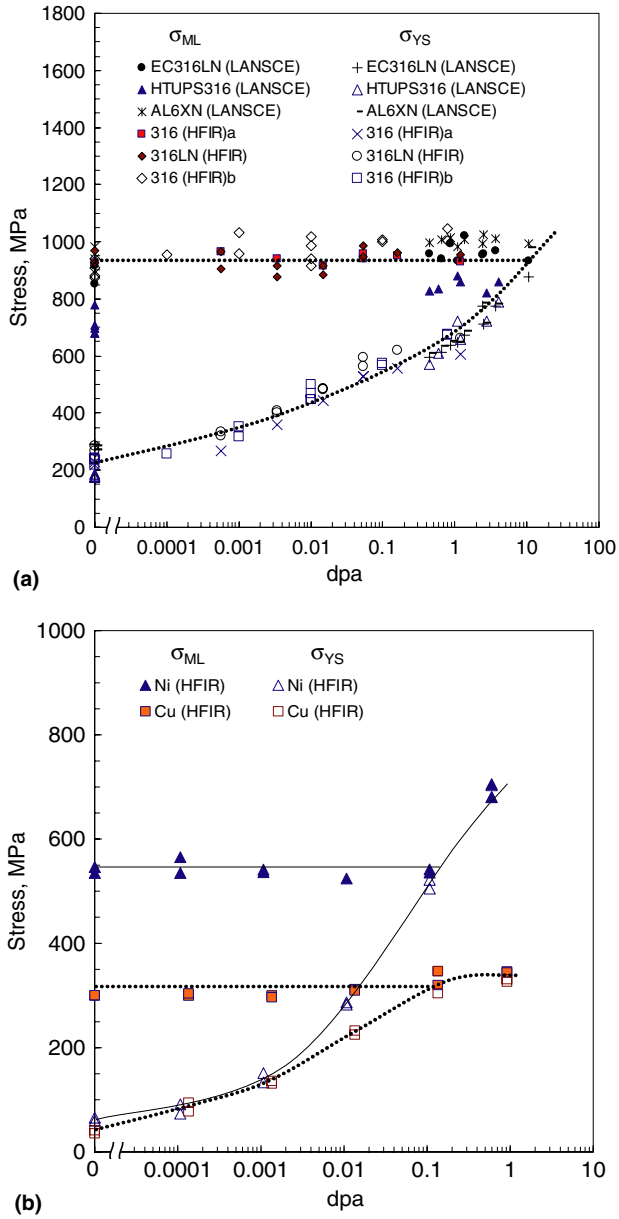

Fig. 5. (a) Dose dependence of the plastic instability stress and yield stress of austenitic stainless steels. (b) Dose dependence of the plastic instability stress and yield stress of pure fcc metals.

$$\sigma_{YS} = \sigma_{ML} \quad \text{for } D > D_C \quad (\sigma_{IS}\text{is not defined in this region}). \tag{3c}$$

These relationships are also indicated in Fig. 4(a) and are applied to all the metallic materials discussed in this report.

Fig. 4(b) shows the dose dependences of σ_{YS} and σ_{ML} for 3Cr and 9Cr steels, including two alloys irradiated in both neutron and spallation irradiation conditions. For the 3Cr and 9Cr steels, the dose dependences of the stresses were similar to those in A533B steel. σ_{IS} was nearly constant at 700–800 MPa. The D_C values for the

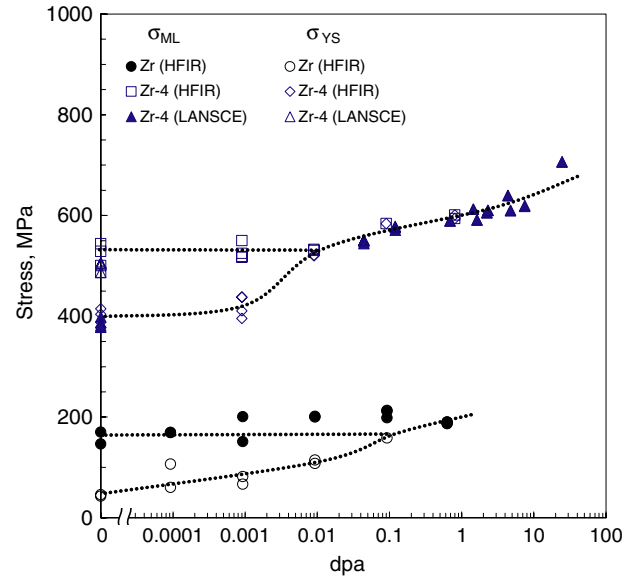

Fig. 6. Dose dependence of the plastic instability stress and yield stress of hcp metals.

3Cr and 9Cr steels were higher than those of the A533B steel; they were: 0.03 dpa for neutron-irradiated 3Cr–3WV steel, and 0.05 dpa for neutron-irradiated 9Cr–1MoVNb, 9Cr–2WV, and 9Cr–2WVTa steels. Further, the D_C values for 9Cr–1MoVNb and 9Cr–2WVTa steels after irradiation in the spallation condition were 0.09 and 0.12 dpa, respectively.

A close look into the difference between σ_{YS} and σ_{ML} ($= \sigma_{ML} - \sigma_{YS}$), which is a measure of the stress range supporting uniform ductility, reveals that in some cases they are not close to each other even at doses higher than D_C. A continuous yielding may account for the above-zero uniform ductility at or above D_C, where other alloys show identical values for σ_{YS} and σ_{ML}. No yield perturbation was found in the 3Cr and 9Cr steels before and after irradiation [7,18]; the transition from elastic to plastic deformation was a continuous process covering a measurable strain range. This continuous yielding is known to occur when stress distribution is inhomogeneous throughout the constituents of the material; yielding begins from high stress zones at an applied stress lower than the nominal yield stress of the material and then spreads to lower stress zones [19]. In the complex, lath structures of the quenched-and-tempered steels [18], an inhomogeneous stress distribution is believed to occur because of the residual stresses (dislocations) after the quenching–tempering process and the misfit stresses between laths during elastic and plastic deformations. In such a case micro-yielding might occur over a significant strain range without a distinct yield point, producing a rounded stress–strain curve close to the 0.2% offset yield point. Since the continuous yielding always gives a positive strain-hardening rate, it has a tendency for delaying plastic

Table 3
Values for true plastic instability stress and dose to plastic instability at yield

#	Materials	Dose range (dpa)	σ_{IS0} (MPa)	σ_{IS} (average over the dose range 0–D_C) (MPa)	D_C (dpa)
1	A533B-a	0–0.89	715	732	0.02
2	A533B-b	0–1.2	665	680	0.015
3	A533B-c	0–1.28	670	678	0.02
4	3Cr–3WV	0–1.2	707	705	0.025
5	9Cr–1MoVNb	0–1.2	748	752	0.034
6	9Cr–2VWTa	0–1.2	764	783	0.054
7	9Cr–2WV	0–1.2	753	768	0.054
8	9Cr–2VWTa	0–10.2	773	802	0.12
9	Mod. 9Cr–1Mo	0–10.2	745	767	0.09
10	Fe-a	0–0.79	304	306	0.2
11	Fe-b	0–1.07	291	291	6
12	Nb	0–0.37	368	368	0.007
13	V	0–0.69	397	393	0.0017
14	316-a	0–0.78	901	975	27
15	316-b	0–1.2	925	941	35
16	316LN	0–1.2	948	935	40
17	EC316LN	0–10.7	883	948	22
18	HTUPS316	0–10.7	709	785	5
19	AL6XN	0–10.7	961	996	17
20	Cu	0–0.92	300	303	0.12
21	Ni	0–0.6	541	530	0.15
22	Zr-4-a	0–0.8	512	524	0.009
23	Zr-4-b	0–24.6	500	500	0.004
24	Zr	0–0.63	159	173	0.09

instability. Even at doses above D_C, small uniform elongations, mostly less than 1%, were detected between the 0.2% offset yield point and the following maximum strength point.

The dose dependencies of σ_{YS} and σ_{ML} for pure bcc metals were not very different from those of bcc alloys, as seen in Fig. 4(c). In spite of large differences in σ_{YS}, the σ_{IS} values were in a narrower range of 290–400 MPa. Relatively low D_C values of 0.007 and 0.002 dpa, respectively, were measured for niobium and vanadium; high impurity levels in these metals may account for relatively high strengths and low D_C values. The values for pure iron were the highest among the bcc metals; 0.2 dpa was measured for Fe-a case and about 6 dpa was estimated for Fe-b case. A high D_C value for the latter case is believed to originate from its high purity (99.995%) and low yield stress. (Lower yield stress before irradiation needs greater irradiation hardening to reach σ_{IS}, which is less dependent on impurity level.)

Figs. 5(a) and (b) present the dose dependencies of σ_{YS} and σ_{ML} for austenitic stainless steels and pure fcc metals, respectively. The dose independence of σ_{IS} was found in all fcc metals; over the dose range 0–D_C the σ_{IS} values were in the range 800–1000 MPa for the stainless steels and about 300 and 540 MPa for copper and nickel, respectively. In the stainless steels, the difference between σ_{YS} and σ_{ML} (or σ_{IS}) is quite large over a large dose range below D_C because of their high strain-hardening capability. The D_C values for the stainless steels were in the range 5–40 dpa. HTUPS316 steel gave the lower end of 5 dpa, but others gave at least 17 dpa for D_C. Also, the D_C values for fcc pure metals, nickel and copper, were 0.15 and 0.12 dpa, respectively. Fig. 6 shows the stress versus dose data for hcp metals. Zircaloy-4-a had a plastic instability stress σ_{IS} of about 510 MPa, while pure zirconium had a small value of 170 MPa. Their D_C values were 0.009 and 0.09 dpa, respectively.

As stated above, the plastic instability stress, σ_{IS}, was approximately independent of dose over the dose range 0–D_C, and the specimen experienced plastic instability when the true stress reached σ_{IS}. This indicates that the earlier observations on the dose independence of σ_{IS} in the austenitic stainless steels [5] and in a vanadium alloy [20] are not alloy-specific phenomena. Further, it is known that unirradiated molybdenum samples pre-strained at a low temperature of 20 °C can develop a plastic instability at yield at an elevated temperature of 220 °C, at which the yield stress of the pre-strained material is higher than the σ_{IS} of a pristine specimen [21,22]. Aluminum [23] also showed work softening (in engineering stress units) and a sharp yield drop when a crystal was deformed at room temperature after heavy cold work at a low temperature of −106 °C. These observations indicate that plastic instability will occur whenever the true stress reaches the σ_{IS} value of pristine material and that the stress at the occurrence of the plastic instability is the same whether strengthening

occurs by prestraining or by irradiation. These observations also imply that the plastic instability process, and probably the strain-hardening process too, is mostly determined by the matrix properties of material, not by the barriers to dislocation glide. This suggests that the uniaxial plastic instability stress, σ_{IS}, should be regarded as a material constant.

3.3. Strain-hardening behavior after irradiation

The loss of uniform ductility after irradiation, prior to necking, has been explained by the reduction of strain-hardening rate or the softening effect due to the clearance of radiation-induced defects by glide dislocations [12,20,24–34]. This may be a possible explanation for the loss of ductility when the strain-hardening behaviors are compared at an equal 'strain' level. However, it has also been suggested that this explanation for the loss of ductility may lead to a wrong conclusion in the interpretation of the effectiveness of radiation-induced defects on strain hardening. Mogford and Hull [13] and Ohr [2] found that the strain-hardening portions of the flow curves for a material after irradiation to various doses were very similar if compared at the same 'stress' level, and therefore that they can be superimposed on the curve for unirradiated material by shifts along the strain axis. Recently, DiMelfi et al.'s results [35] confirmed the dose independence of strain-hardening behavior in neutron-irradiated iron-based alloys such as A212B, A350, Fe–0.28Cu, and Fe–0.74Ni (in wt.%). It was suggested that neutron irradiation has a similar effect as plastic strain on the strain-hardening rate [13]. In the present study, the validity of this suggestion is tested by applying the shifting operation to A533B, EC316LN, and Zircaloy-4 alloys, as representative materials for bcc, fcc, and hcp crystal structures, respectively.

Fig. 7 shows that two true stress–true strain curves for neutron-irradiated A533B steel are superimposed well on the curve for the unirradiated material. The two curves for irradiated material were shifted on the positive true strain axis by strains of 0.035 and 0.09 at 0.003 and 0.015 dpa, respectively. These strains were selected because they provided the best fit with the flow curve of unirradiated material; however, there is the physical significance that these shifts in strain correspond to the shifts in stress from the yield stress of unirradiated material by the amount of irradiation hardening, $\Delta\sigma_{YS}$. On the superimposed portions, the strain-hardening rates of the irradiated specimens were nearly the same as those of the unirradiated material; the flow curve after irradiation represents part of the curve for the unirradiated material. Also note that the plastic instability stresses are comparable for all specimens within experimental error when the strain shifts are adopted. These indicate that the radiation-induced defects do not significantly change the strain-hardening behavior of the

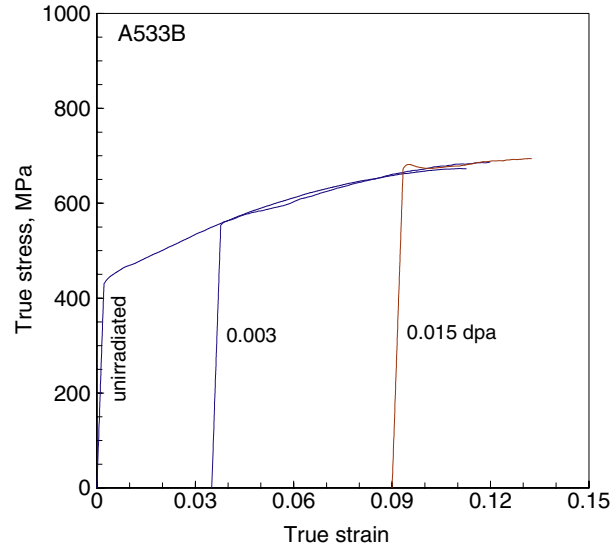

Fig. 7. True stress–true strain curves for A533B steel; the curves of irradiated specimens are shifted in the positive direction by strains of 0.035 and 0.09, respectively, to superimpose on the curve of unirradiated material. Irradiation-induced increases in yield stress were 132 and 235 MPa, respectively.

material. These observations also confirm Mogford and Hull's suggestion [13] that there is an analogy between neutron irradiation and plastic deformation. Comparing the plastic deformation of an irradiated specimen near the yield point with that of an unirradiated specimen that has been strain-hardened to the yield stress level of the irradiated specimen, the defect structures in those two specimens must be different; one includes radiation-induced defects and the other dislocation tangles. However, the observations described here imply that these different defect structures give rise to almost the same strain-hardening behaviors, which in turn implies that only the applied true stress matters in strain hardening. Also, this can be a basis for a suggestion that the dislocation-dislocation interactions, and the dislocation-defect cluster interactions, produce similar net hardening effects if deformations are under the same stress level, even though the details of the interaction mechanisms might be different.

In Fig. 8, the true stress–true strain curves for EC316LN stainless steel after spallation irradiation are superimposed on the curve for unirradiated material. It was noted that at high stresses above 700 MPa the true stresses after irradiation were slightly higher than those of unirradiated material. At least, there was no indication of the 'softening effect' from the radiation-induced defects, which is expected to occur by clearance of defects in irradiated austenitic stainless steels [15,27–30]. In Fig. 9, the curves of irradiated Zr-4 are satisfactorily superimposed on the curve of unirradiated material.

Since the strain-hardening behavior should be related to the deformation mechanism, it seemed worthwhile to

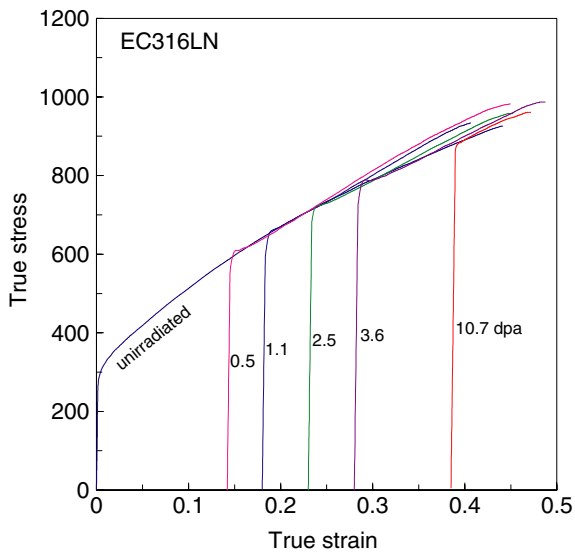

Fig. 8. True stress–true strain curves for EC316LN stainless steel; the curves of irradiated specimens are shifted in the positive direction by strains of 0.14, 0.18, 0.23, 0.28, and 0.385, respectively, to superimpose on the curve of unirradiated material. Irradiation-induced increases in yield stress were 305, 358, 421, 485, and 587 MPa, respectively.

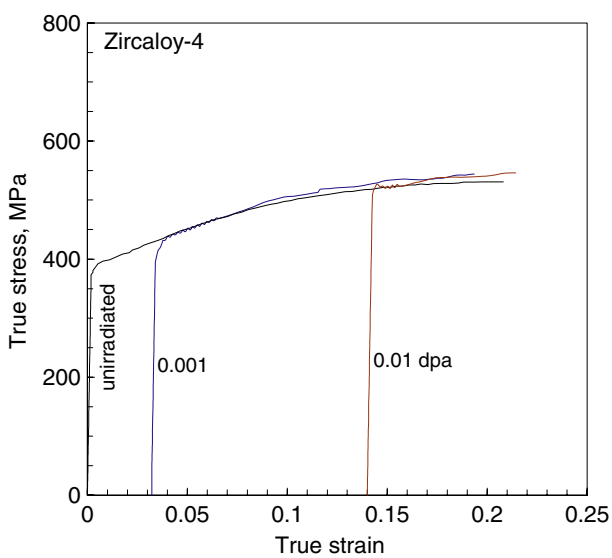

Fig. 9. True stress–true strain curves for Zircaloy-4; the curves of irradiated specimens are shifted in the positive direction by strains of 0.032 and 0.14, respectively, to superimpose on the curve of unirradiated material. Irradiation-induced increases in yield stress were 60 and 132 MPa, respectively.

check whether the initiation of channel deformation is related to D_C. In Table 3, the D_C value ranges widely from 0.0017 to 40 dpa. It is believed that the number-density of radiation-induced defects reaches a saturation level at a significant dose, and channel deformation occurs at or before such saturation [16,24–26,36]. Channel deformation is known to occur well below D_C in fcc metals; for example, in austenitic stainless steels it occurs around 0.1 dpa [16], in nickel at 0.01 dpa [26,37], in gold at 0.001 dpa [26], and in copper at 0.002 dpa [24,25,38]. These doses for channel deformation are 1/100 to 1/10 of their D_C values. In bcc and hcp alloys, channel deformation has been observed to occur at around their D_C values [16,37]; however, more investigation is necessary for generalization of the postulated relationship between D_C and the critical dose for saturation in irradiation hardening. Whether the saturation in irradiation hardening occurs simultaneously with channel deformation or not seems to depend on the material properties, especially on the ductility and strain hardening capability before irradiation. If hardening by radiation-induced defect clusters and hardening by prestrain (dislocations) have similar effects, then a connection with saturation of defect clusters would also imply a similar saturation with prestrain.

3.4. Suggested explanations for the dose independence of strain-hardening behavior

Although it is evident that channel deformation can occur at or below D_C, no softening effect from channels is observed in the dose range 0–D_C if true stress–true strain curves are compared at equal stress levels. Indeed, no negative strain-hardening rate or strain softening was measured in previous studies even during necking deformation [6,20]. These observations indicate that the true strain-hardening rate is not affected by the change in deformation mechanism from dislocation tangling to dislocation channeling induced by irradiation. An apparent reduced strain-hardening rate is displayed by the true stress–true strain curve of irradiated material because the flow curve corresponds to the high-strain portion of the curve for unirradiated material, which has a reduced strain-hardening rate. To explain the dose independence of strain-hardening behavior, we suggest two possible reasons: (1) Similar true strain-hardening behaviors can be produced by the channel deformation in irradiated materials and by the uniform deformation in unirradiated materials. (2) Deformations in irradiated materials and in heavily deformed unirradiated materials are both equally localized.

If the first suggestion is correct, the strain-hardening rate due to the long-range back stresses in the channels in irradiated metals should be as high as that in the region of uniform deformation in unirradiated metals. Although the detailed mechanism of channel formation is largely unknown, a number of studies have confirmed that defect clusters are cleared within the channels [10–12,24–34,38]. A significant drop of local shear stress in the channel should occur because of this clearance in the early stage of channel formation; however, the local stress should return quickly to a stress level as high as those in adjacent regions as the back stress builds up

[39,40]. Actually, as long as the channel formation spreads to adjacent regions, the local strain-hardening rate cannot be negative. This is because a negative strain hardening will cause immediate local instability without forming a diffused necking which can give rise to a large necking ductility. However, most of the test metals retained significant necking ductility, even with prompt necking at yield [10,38,41]. No negative slope in the true stress–true strain curve has been calculated for the necking deformation after significant irradiation [6,20]. Some of the dislocations generated during channel formation may form pileups against strong obstacles, such as grain boundaries, without being transferred across the boundaries, and the back stress due to the dislocation pileups might stop further slip in the channel [39,40]. This might be true because the vector sum (total displacement vector) of the Burgers vectors of channeling dislocations may not be fully resolved by propagation of the channel into the next grain when any misorientation exists between grains [40]. The unresolved displacement component should be accommodated in a form of an unresolved strain component, like dislocation pileups and elastic strains at grain boundaries. Also, if a gradual increase in the number of channels is assumed, either a contribution to the macroscopic stress, or a softening effect by means of the growing channels, should be relatively small, because the volume affected by the channels under their formation might be only a small fraction of the total load-bearing volume. Thus, only channels formed early might lead to negative strain hardening, causing a yield drop [33,41]. However, the strain-hardening rate after early deformation might again become positive because individual pileups formed by localized dislocation glides at the channel-grain boundary intersections may be larger than those formed in uniform deformation [39–41]. A positive macroscopic strain-hardening rate as high as that in uniform deformation may be achieved by a small number of large pileups if the average back stress from those pileups is as high as that from more uniformly distributed smaller pileups in uniform deformation.

There is also supporting evidence for the second suggestion. Localized (channeled) deformation has been reported for unirradiated, pre-strained Cu [42–45], Mo [10,21,22], Al [23], and dispersion hardened materials [46]. In these results, macroscopic strain-hardening rates were positive, although localized (channeled) deformation was observed or predicted. These results suggest that localized (or channeled) deformation is a common phenomenon at high stresses, whether the material is irradiated or not. Possible mechanism to initiate microscopic strain localization could be a local softening effect due to dislocation annihilation (or dynamic recovery), which is analogous to the defect clearing process in irradiated materials. After a large deformation, there is a high probability that dislocation–dislocation interactions can cause annihilation, and the dislocation annihilation might accelerate as the dislocation density increases [47,48]. This agrees with the observation that channel deformation can be observed in materials after strengthening by any measures [10–12,24–34,42–45]. It is seen most readily in transmission electron microscopy examination of irradiated materials because the radiation damage microstructure provides a sharp contrast backdrop to the cleaned channels. It is more difficult to detect in prestrained materials because of lack of contrast. If the strain localization concept as a high stress phenomenon is correct, a higher tendency for strain localization should be observed in any high stress deformations, such as high speed deformations and low temperature deformations. It should become a significant factor in nanostructured materials where yield strengths are considerably increased.

Although the present data are not enough to generalize either of the above explanations for the dose independence of strain-hardening behavior, the present results supply evidence that channeling (or localized deformation) occurs more easily in high stress and low strain-hardening rate conditions. A study is ongoing for confirmation of these suggestions.

4. Conclusions

Plastic instability behavior and its relationship with irradiation hardening have been analyzed for polycrystalline metals including ten bcc, seven fcc, and two hcp metals after irradiation at low temperatures (<200 °C). Conclusions drawn from the analysis are given as follows:

1. The engineering tensile curve after irradiation showed necking at yield when the yield stress was above the plastic instability stress of unirradiated material. It was also shown that the plastic instability stress prior to necking at yield, σ_{IS}, is approximately independent of dose. These observations are believed to be general phenomena for hardened metallic materials, at least after low temperature irradiation.
2. Macroscopic plastic instability occurred at yield when the irradiation dose exceeded a critical level, defined as the dose to plastic instability at yield, D_C. The D_C values ranged from 0.002 to 0.2 dpa for bcc and hcp metals except high purity iron. The high purity iron gave a high D_C of 6 dpa. D_C ranged from 0.1 to 40 dpa for fcc metals. The low D_C values for niobium and vanadium may be due to their high yield stresses.
3. It was verified that the true stress–true strain curves for irradiated materials can be superimposed well on the curves for unirradiated materials by shifting along the strain axis. This suggests that two different defect

structures, radiation-induced defects and deformation-produced dislocations, result in similar net effects on strain-hardening behavior.

4. For the dose independence of strain-hardening behavior, two possible explanations were suggested: (1) Similar strain-hardening behaviors are produced by channel deformation in irradiated materials and the uniform deformation in unirradiated materials. A strong back stress buildup in the channels is needed for this explanation to be valid. (2) The deformations in irradiated and unirradiated materials are equally localized at equal true stress. The dislocation annihilation phenomenon in unirradiated materials, which is analogous to defect clearing in irradiated materials, might play a major role in strain localization.

Acknowledgements

This research was sponsored by US Department of Energy, Offices of Fusion Energy Sciences and Basic Energy Science, under Contract DE-AC05-00OR22725 with UT-Battelle, LLC. The authors express special thanks to Drs. J.G. Merkle and R.L. Klueh for their technical reviews and thoughtful comments.

References

[1] Pawel JE, Rowcliffe AF, Alexander DJ, Grossbeck ML, Shiba K. J Nucl Mater 1996;233–237:202.
[2] Ohr SM. Scripta Metall 1968;2:213.
[3] Lucas GE, Billone M, Pawel JE, Hamilton ML. J Nucl Mater 1996;233–237:207.
[4] Farrell K, Byun TS. J Nucl Mater 2001;296:129.
[5] Byun TS, Farrell K, Lee EH, Hunn JD, Mansur LK. J Nucl Mater 2001;298:269.
[6] Byun TS, Farrell K, Lee EH, Mansur LK, Maloy SA, James MR, Johnson WR. J Nucl Mater 2002;303:34.
[7] Farrell K, Byun TS. J Nucl Mater 2003;318:274.
[8] Byun TS, Farrell K. J Nucl Mater 2003;318:292.
[9] Odette GR, He MY, Donahue EG, Lucas GE. On the relation between engineering load–displacement curves and true stress–strain behavior in test of flat tensile specimens. In: Sokolov MA, Landes JD, Lucas GE, editors. Small specimen test techniques: fourth Volume, ASTM STP 1418. West Conshohocken, PA: American Society for Testing and Material; 2002. p. 221.
[10] Luft A. Microstructural processes of plastic instabilities in strengthened metals. Progr Mater Sci 1991;35:97.
[11] Smidt Jr FA. Dislocation channeling in irradiated metals, NRL Report 7078, Naval Res. Lab., Washington DC; 1970.
[12] Wechsler MS. Dislocation channeling in irradiated and quenched metals. In: The inhomogeneity of plastic deformation. Metals Park, OH: American Society for Metals; 1971. p. 19.
[13] Mogford IL, Hull D. J Iron Steel Inst 1963;201:55.
[14] Farrell K, Byun TS. Tensile properties of candidate SNS materials after irradiation in two neutron areas in the LANSCE accelerator, SNS/TR-211. Oak Ridge National Lab; 2001.
[15] Maloy SA, James MR, Willcutt G, Sommer WF, Sokolov M, Snead LL, Hamilton ML, Garner F. J Nucl Mater 2001;296:119.
[16] Farrell K, Byun TS, Hashimoto N. Mapping flow localization processes in deformation of irradiated reactor structural alloys. Oak Ridge National Lab., ORNL/TM-2003/63; 2003.
[17] Dieter GE. Mechanical metallurgy. 3rd ed. McGraw-Hill; 1986.
[18] Klueh RL, Harries DR. High-chromium ferritic and martensitic steels for nuclear applications. Conshohocken, PA: American Society for Testing and Material; 2002.
[19] Sakaki T, Sugimoto K, Fukuzato T. Acta Metall 1983;31:1737.
[20] Van Osch EV, DeVries MI. J Nucl Mater 1991;271&272:162.
[21] Brenner B, Luft A. Mater Sci Eng 1982;52:229.
[22] Ritschel C, Luft A, Schulze D. Kristall und Technik 1978;13:791.
[23] Cottrell AH, Stokes RJ. Proc Roy Soc A 1955;233:17.
[24] Sharp JV. Acta Metall 1974;22:449.
[25] Sharp JV. Philos Mag 1967;16:77.
[26] Okada A, Kanao K, Yoshiie T, Kojima S. Mater Trans JIM 1989;30:265.
[27] Suzuki M, Sato A, Mori T, Nagakawa J, Yamamoto N, Shiraishi H. Philos Mag 1992;65:1309.
[28] Song SG, Cole JI, Bruemmer SM. Acta Mater 1997;45:501.
[29] Suzuki M, Sato A. J Nucl Mater 1990;172:97.
[30] Cole JI, Bruemmer SM. J Nucl Mater 1995;225:53.
[31] Tucker RP, Wechsler MS, Ohr SM. J Appl Phys 1969;40:400.
[32] Norwood DO, Gilbert RW, Coleman CE. Effect of stress on radiation damage in neutron irradiated zirconium alloys. In: Lowe Jr AL, Parry GW, editors. Zirconium in the nuclear industry, ASTM STP 633. West Conshohocken, PA: American Society for Testing and Material; 1977. p. 418.
[33] Onchi T, Kayano H, Higashiguchi Y. J Nucl Mater 1980;88:226.
[34] Adamson RB, Wisner SB, Tucker RP, Rand RA. Failure strain for irradiated Zircaloy based on subsized specimen testing and analysis. In: Corwin WR, Lucas GE, editors. The use of small specimens for testing irradiated material, ASTM STP 888. West Conshohocken, PA: American Society for Testing and Material; 1986. p. 171.
[35] DiMelfi RJ, Alexander DE, Rehn LE. J Nucl Mater 1998;252:171.
[36] Eldrup M, Singh BN, Zinkle SJ, Byun TS, Farrell K. J Nucl Mater 2002;307–311:912.
[37] Byun TS, Farrell K. Irradiation hardening behavior of polycrystalline metals after low temperature irradiation. J Nucl Mater [in press].
[38] Singh BN, Edwards DJ, Toft T. J Nucl Mater 2001;299:205.
[39] Makin MJ, Sharp JV. Phys State Solid 1965;9:109.
[40] Gittus J. Irradiation effects in crystalline solids. Applied Science Publisher; 1978.
[41] Singh BN, Foreman AJE, Trinkaus H. J Nucl Mater 1997;249:103.
[42] Sharp JV, Makin MJ. Can J Phys 1967;45:519.
[43] Basinski ZS, Jackson PJ. Appl Phys Lett 1965;15:148.
[44] Basinski ZS, Jackson PJ. Phys State Solid 1965;9:805.
[45] Basinski ZS, Jackson PJ. Phys State Solid 1965;10:45.
[46] Mori T, Mura T. Mater Sci Eng 1976;26:89.
[47] Polyzos B, Douka E. Trochidis. J Appl Phys 2001;89:2124.
[48] Flinn JE, Field DP, Korth GE, Lillo TM, Macheret J. Acta Mater 2001;49:2065.